Online Identification of Pilot Adaptation to Sudden Degradations in Vehicle Stability

Plaetinck, Wouter; Pool, Daan; van Paassen, Rene; Mulder, Max

DOI
10.1016/j.ifacol.2019.01.020

Publication date
2019

Document Version
Final published version

Published in
IFAC-PapersOnLine

Available online at www.sciencedirect.com

ScienceDirect

IFAC Papers Online CONFERENCE PAPER ARCHIVE

IFAC PapersOnLine 51-34 (2019) 347–352

Online Identification of Pilot Adaptation to Sudden Degradations in Vehicle Stability

W. Plaetinck, D.M. Pool, M.M. van Paassen and M. Mulder *

* *Control and Simulation Section, Aerospace Engineering, Delft University of Technology, 2629 HS, Delft, The Netherlands (e-mail: d.m.pool@tudelft.nl).*

Abstract: Time-varying pilot control identification is essential for better understanding of how pilots respond when faced with sudden changes in the dynamics of the vehicle they control, such as when automatic control and stabilization systems disengage or undergo a mode transition. This paper presents the results of a human-in-the-loop experiment performed at TU Delft to test a promising online pilot identification method, based on recursive low-order ARX identification, developed in earlier work. In the experiment, eight skilled participants performed tracking tasks with time-varying vehicle dynamics, where at an unpredictable moment during each tracking run a sudden degradation in vehicle stability was induced. In addition to controlling the time-varying vehicle, participants were asked to indicate when they detected the change in the vehicle dynamics with a button push. This paper compares the effectiveness of two different approaches to detect the moment when pilot adaptation occurs from online identified pilot parameter traces. Overall, the results indicate that the lag in this detection of identified pilot adaptation is equivalent to the subjective detection times, or less. This implies that these online techniques have clear potential for ensuring timely and effective changes in adaptive pilot support systems.

1. INTRODUCTION

While most of our current knowledge about how pilots control dynamics systems is valid only for time-invariant task conditions (McRuer and Jex, 1967), it is in fact pilots' capacity for quick, time-varying, control adaptations that is of critical importance for many real-life control tasks (Young, 1969; Mulder et al., 2018). Of special interest in the aerospace domain are pilots' interactions with time-varying controlled vehicle dynamics, which for instance may occur due to aircraft damage and sudden autopilot or stabilization system mode switches or disengagement (Hess, 2009, 2016; Zaal, 2016; Farjadian et al., 2016). Due to the often safety-critical nature of such cases, which can require significant time-varying pilot adaptation, a better quantitative understanding of the nature of such adaptations is needed (Mulder et al., 2018). Furthermore, accurate *online* detection and characterization of time-varying pilot adaptations – i.e., *in real time* – has great potential for, for instance, the detection of reduced attention or distraction and the design of adaptive pilot support systems and interfaces.

Traditionally, two perspectives on quantitative analysis of time-varying pilot behavior are followed: the development and testing of empirically-derived logic rules for the adaptation (Hess, 2009, 2016; Farjadian et al., 2016), or the explicit identification, using system identification methods, from collected pilot-in-the-loop data. For the latter, significant progress has been made towards developing time-varying identification methods suitable for offline, *a posteriori*, identification: e.g., methods based on Kalman filters (Schiess and Roland, 1975; Boer and Kenyon, 1998; Popovici et al., 2017), wavelets (Thompson et al., 2001), linear parameter varying (LPV) models (Duarte et al., 2017), or explicit modeling of time-variations (Zaal, 2016). In the current state-of-the-art, however, a validated online identification approach, together with a tested algorithm for detecting pilot adaptations from identified time-varying parameter traces, is still missing.

In this paper, a previously developed recursive ARX identification technique (van Grootheest et al., 2018) is implemented *in real time* and tested for its capacity to *online* identify, and timely detect, time-varying pilot adaptation in response to a sudden degradation in vehicle stability. To test the method, a dedicated human-in-the-loop experiment was performed, similar to (Zaal, 2016), where eight participants performed tracking tasks with time-varying controlled element (CE) dynamics. To detect HC adaptation from identified traces of pilot response gains, two different detection methods were tested, which compared current values of these identified parameters against either an *a priori* estimated time-invariant condition average, or a moving average of the identified trace itself. For comparison with the identified adaptation detections, participants in the experiment were also asked to indicate, by means of a button push, when they detected a change in the CE dynamics during the tracking task.

2. METHOD

2.1 Control Task

A single-axis compensatory tracking task, based on the experiment of Zaal (2016), was used to evaluate the time-varying pilot identification and adaptation detection methods. A block diagram of this task is shown in Fig. 1. In this task, the pilot controls the time-varying controlled element (CE) dynamics $H_c(s,t)$ such that its output y

2405-8963
Peer review under responsibility of International Federation of Automatic Control.
10.1016/j.ifacol.2019.01.020

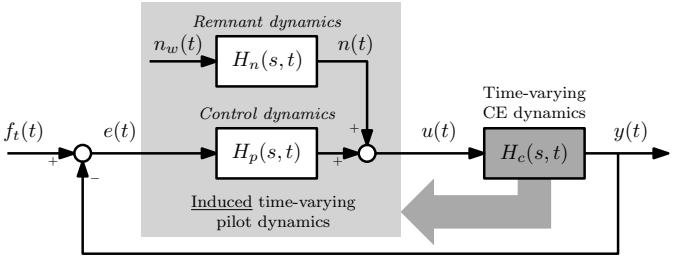

Fig. 1. A schematic representation of a pilot in control of time-varying CE dynamics.

tracks the forcing function f_t as closely as possible. The pilot minimizes the tracking error e, as presented on a compensatory display, and provides a single control input to the CE, u. In line with traditional quasi-linear pilot modeling assumptions (McRuer and Jex, 1967), in this task both the linear control dynamics $H_p(s,t)$ and the characteristics of the nonlinear remnant contribution $H_n(s,t)$ are expected to vary due to a change in the CE. For the CE, a typical low-order approximation of aircraft dynamics is considered:

$$H_c(s,t) = \frac{K_c(t)}{s^2 + \omega_c(t)s} \tag{1}$$

To induce time-varying pilot adaptation, the parameters of the CE dynamics in Eq. (1) – i.e., the gain K_c and the break frequency ω_c – were changed over time. To tie in with (Zaal, 2016), a sigmoid function was used to vary both parameters between an initial (i.e., subscript "1") and a final (i.e., "2") value, e.g., $K_c(t) = K_{c_1} + (K_{c_2} - K_{c_1})/(1 + e^{-G(t-M)})$. The initial CE dynamics represent a highly stable and responsive vehicle, while the final CE dynamics are notably less stable and more sluggish and require pilots to generate lead (McRuer and Jex, 1967). As shown in Fig. 2, two different settings of the sigmoid rate of change parameter G were considered, 0.5 and 100 s^{-1}, to include both instantaneous and more gradual changes in the CE. For consistent data collection, the CE variation was always centered on the midway point of the measurement interval $T_m = 81.92$s, i.e, $M = 40.96s$.

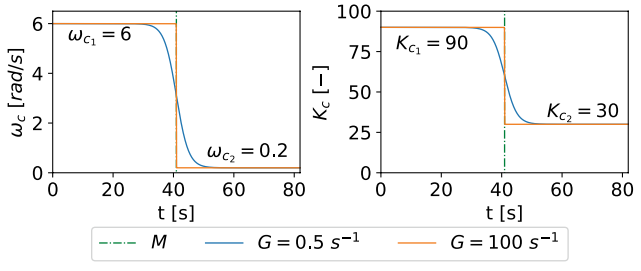

Fig. 2. CE parameters scheduled by sigmoid function for a sudden ($G = 100$ s^{-1}) and a gradual change ($G = 0.5$ s^{-1}), located at $M = T_m/2$.

2.2 Pilot Model

For the considered time-varying control task, it is known that the time-varying pilot control dynamics $H_p(s,t)$ are effectively quantified with a traditional linear pilot model for which (part of) the parameters are free to vary over time (Zaal, 2016; Duarte et al., 2017; van Grootheest et al., 2018), see Eq. (2). Note that to avoid identification ambiguities between the error response gain K_e and the lead time constant T_L normally present in models of this form (McRuer and Jex, 1967), an error rate response gain $K_{\dot{e}}(t) = K_e(t)T_L(t)$ is used for the parameterization:

$$H_p(s,t) = (K_e(t) + K_{\dot{e}}(t)s)e^{-s\tau}H_{nm}(s,t) \tag{2}$$

$$H_{nm}(s,t) = \frac{\omega_{nm}^2(t)}{\omega_{nm}^2(t) + 2\zeta_{nm}(t)\omega_{nm}(t)s + s^2} \tag{3}$$

As previous work has found no evidence for time-varying adaptations of the pilot response delay τ (Zaal, 2016) for the considered scenario, four time-varying pilot parameters are estimated. The pilot gains $K_e(t)$ and $K_{\dot{e}}(t)$ capture how much proportional and derivative control is performed by pilots. The natural frequency ω_{nm} and damping ratio ζ_{nm} of the neuromuscular dynamics $H_{nm}(s,t)$ (see Eq. (3)) account for time-varying neuromuscular adaptations.

2.3 Online Time-Varying ARX Identification

The goal of time-varying pilot identification is to use measured time traces of the tracking error e and the control signal u (see Fig. 1) to estimate time traces of all time-varying pilot model parameters. In this paper, for this a previously developed approach based on the "autoregressive with external input" (ARX) model structure is applied (van Grootheest et al., 2018).

ARX Model Structure Eq. (4) gives the general single-input-single-output ARX model structure (Ljung, 1999) that is used in this paper:

$$u(t) = \frac{B(q)}{A(q)}q^{-n_k}e(t) + \frac{1}{A(q)}\epsilon(t) \tag{4}$$

Eq. (4) represents a discrete-time model with time shift operator q, such that $q^{-n_k}e(t) = e(t - n_k)$ to model the pilot (input) delay. Pilot dynamics are approximated by the ratio $B(q)/A(q)$ of the ARX polynomial models and the input data shift of n_k samples. Eq. (4) shows that the system and noise (remnant) dynamics are coupled through $A(q)$ in the ARX model structure, which makes estimating its parameters a straightforward least-squares problem.

In this paper, second-order $A(q)$ and $B(q)$ polynomials were chosen to match Eq. (2). The resulting ARX model structure of Eq. (5) allows for estimating the vector of polynomial coefficients – i.e., $\theta_i = (a_1\ a_2\ b_0\ b_1)^T$ – with RLS, but not the discrete input time shift parameter n_k. As was shown to be an allowable approximation by van Grootheest et al. (2018), the pilot time delay was set *a priori* to $\tau = 0.28$ s (Zaal, 2016), corresponding to $n_k = 28$ for the 0.01 s timestep considered in the experiment.

$$H_p(q) = \frac{B(q)}{A(q)}q^{-n_k} = \frac{b_0 + b_1q^{-1}}{1 + a_1q^{-1} + a_2q^{-2}}q^{-n_k} \tag{5}$$

Recursive Least Squares An RLS algorithm with standard exponential forgetting factor was used to estimate and track the ARX coefficients over time (Ljung, 1999; van Grootheest et al., 2018). The forgetting factor, for the considered 100 Hz data rate, was set to $\lambda = 0.99609$ based on detailed tuning performed in previous work (van Grootheest et al., 2018). This value corresponds to a memory horizon of 2.56 s. The RLS algorithm estimated θ_i at every sample time step, starting at $i = 3$ s, as at earlier time instances insufficient data over the memory horizon are available, accounting also for the input time shift n_k. To start the RLS, default initial parameter and parameter covariance matrix settings of $\theta_0 = (-1.85\ 0.85\ 0.08\ -0.08)^T$ and $P_0 = 10,000\boldsymbol{I}_{4x4}$, respectively, were used.

Pilot Parameter Retrieval To retrieve the physical pilot parameters from Eq. (2), the estimated discrete-time ARX coefficients need to be converted. This is done by first converting the estimated ARX models to discrete-time transfer functions $H_p(z)$ using the Z-transform. The discrete transfer function estimated at each time step is then converted to the continuous-time equivalent, using a zero-order-hold conversion method. The pilot model parameters can then be retrieved from the converted ARX model parameters using the following relations, where the superscript "c" indicates that the ARX coefficients from Eq. (5) have been converted to continuous time first:

$$\begin{aligned} K_e &= \frac{b_1^c}{a_2^c} & K_{\dot{e}} &= \frac{b_0^c}{a_2^c} \\ \zeta_{nm} &= \frac{a_1^c}{2\sqrt{a_2^c}} & \omega_{nm} &= \sqrt{a_2^c} \end{aligned} \tag{6}$$

It should be noted that this conversion is straightforward as long as the orders of the parameter and ARX models match. Otherwise, an order reduction technique would be required for the parameter retrieval.

2.4 Adaptation Detection

For the considered task, the main expected pilot adaptation is a reduction in the error gain K_e and an increased error rate gain $K_{\dot{e}}$ after the induced drop in vehicle stability (Zaal, 2016). For this reason, this paper tests two adaptation detection methods that perform the detection based on the time-varying estimates of these two parameters. Both proposed detection methods check for instances where the current estimate of the parameter (e.g., $K_{\dot{e}}$) is outside of a range linked to an expected average value (e.g., $\bar{K}_{\dot{e}}$) of the considered parameter and an accepted variability margin (e.g., $\delta K_{\dot{e}}$). This principle is illustrated in Fig. 3, where the blue area indicates the reference average parameter range and the red line indicates the identified parameter trace.

As shown in Fig. 3, two different approaches were tested for defining the reference band, leading to two adaptation detection methods:

- *Time-Invariant Condition Average* (TICA), Fig. 3(a): in this approach the reference parameter variation $\bar{K}_{\dot{e},TICA}$ and spread is defined *a priori* and derived from identified parameter traces of time-invariant task runs, i.e., with only the stable CE dynamics.
- *Moving Average* (MA), Fig. 3(b): in this approach the center of the reference band $\bar{K}_{\dot{e},MA}$ is derived from the current identified parameter trace *only*, by taking a moving average over a past window of n_s samples.

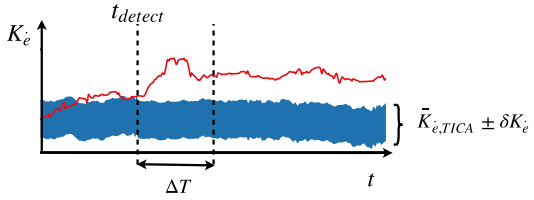

(a) TICA method

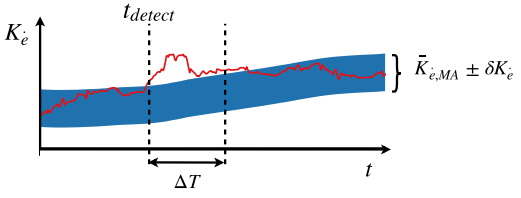

(b) MA method

Fig. 3. Graphical illustration of adaptation detection for both the proposed TICA and MA methods.

Both detection methods have several settings that should be tuned to minimize false-positive and false-negative detections. A false positive (FP) was defined as a detection made outside of the interval $M < t_d < 60$ s, with $M = 40.96$ s the moment of transition. A limit of 60 s was arbitrarily chosen since by then pilots should have adapted to the new situation and the identified parameters should be sufficiently converged to trigger a detection. A false negative (FN) occurs when no detection was made. This, for instance, can happen when the parameter trace is not outside the reference band for longer than ΔT seconds. The tunable settings (hyperparameters) of the detection methods, which should be tuned to avoid FP and FN, are:

- $\delta K_{\dot{e}}$, δK_e: the accepted variability margin size. These parameters define the width of the reference band and quantifies the allowed (or expected) deviation of pilot parameter estimates from the average without leaving the reference band.
- $\bar{K}_{\dot{e}}$, $\bar{K}_e$: the middle of the reference parameter band, defined following a different strategy for the TICA and MA methods, see Fig. 3.
- ΔT: the minimum amount of time the current parameter trace should be outside of the reference band to be considered a detection.
- n_s (for MA method only): the number of samples over which the reference moving-average parameter average is calculated, which directly influences the tracking speed of the moving average.

The TICA approach here is used as a reference, as for general applications detailed knowledge of parameter variations in equivalent time-invariant scenarios are not available. The MA approach requires less additional data to tune and is thus more promising for online implemen-

tation. In this paper, both methods are applied to the identified traces of both K_e and $K_{\dot{e}}$.

3. EXPERIMENT SETUP

3.1 Apparatus

To evaluate the proposed methodology for detecting pilot adaptation to changes in the CE, a dedicated human-in-the-loop experiment was performed where participants performed the control task of Fig. 1. The experiment was performed in the fixed-base simulator setup of the Human-Machine Interaction Laboratory (HMILab) at the Faculty of Aerospace Engineering at TU Delft, see Fig. 4. The control task was implemented as a pitch attitude tracking task matching the experiment of Zaal (2016), where participants were asked to minimize pitch tracking errors shown as the vertical displacement between a (stationary) aircraft symbol and the (moving) horizon line, see Fig. 4(a).

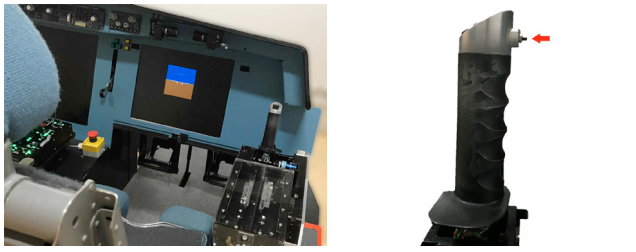

(a) HMILab simulator (b) Stick with push button

Fig. 4. The experiment setup in the HMILab simulator (a) and the push button on control stick (b).

Participants provided their control inputs using a right-handed electro-hydraulic side-stick as shown in Fig. 4(a). The stick's torsional stiffness was set to 2.5 Nm/rad, its damping to 0.22 Nm s/rad, and its inertia to 0.01 kg m^2 with a moment arm of 9 cm. The stick could only rotate around the pitch axis. Finally, a push button on the stick, see Fig. 4(b), was used by the participants to indicate when they detected the change in the task characteristics.

3.2 Forcing Function

The forcing function f_t was defined as a sum of ten sinusoids with different frequencies, all defined as integer multiples of the base measurement frequency $\omega_m = 2\pi/T_m$ to avoid spectral leakage.The forcing function was identical to the signal used by Zaal (2016), however, it was shifted by 10.5 s backwards in time, by an adjustment to the phases. This was done to have a different part of the f_t time trace align with the CE transition region.

3.3 Experiment Conditions

In the experiment, two variables were varied independently and all combinations were tested by all participants (within-subjects design). First, participants were subjected to both fast and gradual time-variations of the CE – referred to as TV12F and TV12S in the remainder of this paper – implemented with two values for the maximum rate-of-change parameter of the sigmoid function: $G = 100$ or 0.5 s^{-1}, respectively, see Fig. 2. In addition,

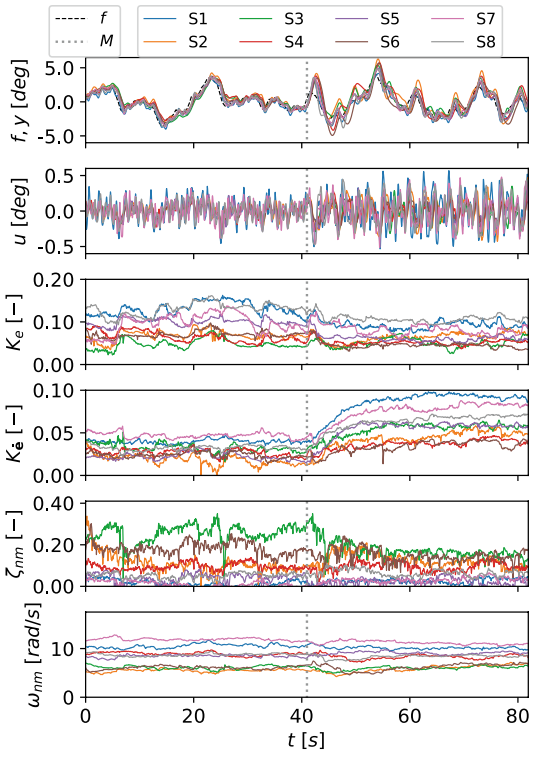

Fig. 5. Measured average pilot control data (f_t, y, and u) and average identified pilot parameter traces (K_e, $K_{\dot{e}}$, ζ_{nm}, and ω_{nm}) for all participants (condition TV12F).

to ensure that the time of the CE change occurred did not become predictable, the amount of run-in time added before the measurement window of $T_m = 81.92$ s was varied over three levels: 5 s, 10 s and 15 s. Finally, time-invariant reference data with the initial CE dynamics ($K_c = 90$, $\omega_c = 6$ rad/s) were also collected for each participant for implementing the TICA adaptation detection.

3.4 Participants and Experiment Procedures

Eight skilled participants volunteered to perform the experiment and provided written informed consent before participating. Participants were instructed to minimize the tracking error shown on the display and push the button whenever they noticed changed CE dynamics. They received no further briefing regarding nature of the tested experiment conditions. After an initial training consisting of at least one run of each condition, three further repeated measurements of each condition were collected for each participant, using a randomized order of presentation to balance out fatigue effects. After each run, participants received feedback of their performance (RMS of the error signal e) as motivation to perform consistently.

4. RESULTS

4.1 Time-Varying Pilot Identification Data

To illustrate the first step of our proposed procedure, Fig. 5 shows average recorded time traces from the control task (f_t, y, and u, see Fig. 1), as well as the time-varying estimates of the four free parameters of the pilot model of Eq. (2) for condition TV12F. As is clear from the top

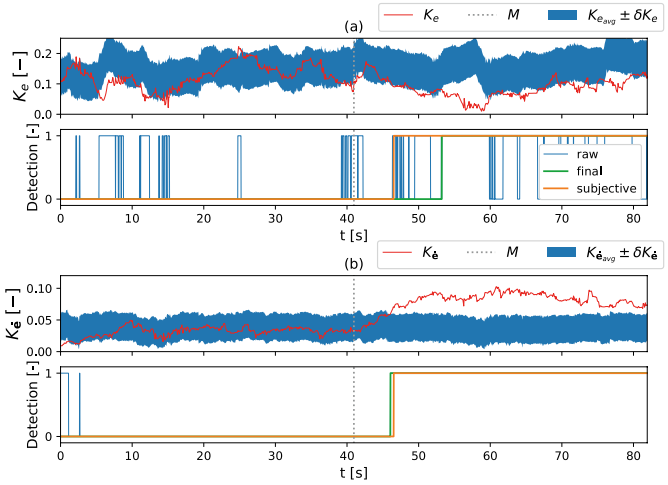

Fig. 6. Adaptation detection using TICA. Hyperparameters: $\delta K_e = 0.06$, $\delta K_{\dot{e}} = 0.02$, $\Delta T = 3$ s.

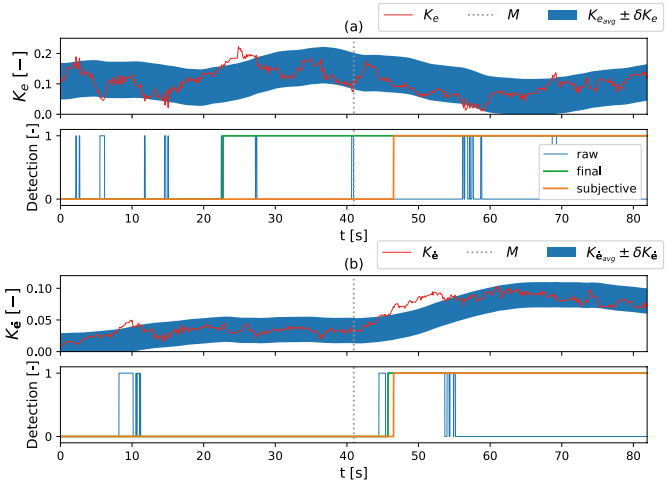

Fig. 7. Adaptation detection using MA. Hyperparameters: $\delta K_e = 0.06$, $\delta K_{\dot{e}} = 0.02$, $\Delta T = 3$ s, $n_s = 1500$.

two graphs, after the CE transition indicated with the dashed vertical line, participants showed degraded tracking performance (less accurate following of f_t with y) and increased control effort (larger u), as expected for a loss of vehicle stability and responsiveness. The estimated pilot parameter traces show the matching expected decrease in K_e and a notable increase in $K_{\dot{e}}$ of up to 100% after the induced CE change (McRuer and Jex, 1967). Fig. 5 also confirms earlier findings (Zaal, 2016; van Grootheest et al., 2018), as also for this data no consistent time-varying adaptations in the neuromuscular parameters are observed.

4.2 Adaptation Detection from Pilot Identification

To demonstrate the adaptation detection performed with the TICA and MA algorithms, Figs. 6 and 7 show example results for a single tracking run of one subject for the condition with a sudden change in the CE, i.e., TV12F. Each figure consists of two sets of graphs – one set for K_e and one for $K_{\dot{e}}$ – and for each set the top graph shows the respective identification data, while the bottom graph shows the derived detection results. Matching Fig. 3, the identified parameter variation over time is the red data, while the parameter range used for the adaptation detection is indicated as a blue area. In the detection graphs, blue data are the "raw" detections that represent all instances when the parameter trace goes outside of the reference band, while the green data indicates the "final" result, i.e., the first detection that has a length longer than ΔT. For reference, the subjective detection (button press) is indicated in red. The results presented here were obtained for an initial heuristic tuning of the hyperparameters for both algorithms, based on inspection of the nature and variability of the identified pilot parameter traces across our dataset.

Figs. 6 and 7 show that adaptation detection based on K_e is more troublesome, as inherent parameter variations unrelated to the CE change seem to be comparatively larger than for $K_{\dot{e}}$. Fig. 7 even shows a clear FP, as only a very early detection well before the actual CE change is triggered for the MA method. For error detection based on $K_{\dot{e}}$, the raw detection data show that both methods are also clearly triggered due to local, short-duration, variations in the identified $K_{\dot{e}}$. However, after taking a minimum ΔT into account, the final result for both is a detection at around 46 s, which is very close to the subjective detection time indicated by this participant.

Table 1. Error detection confusion matrix for both methods. Hyperparameters: $\delta_{K_e} = 0.06$, $\delta_{K_{\dot{e}}} = 0.02$, $\Delta T = 3$ s, $n_s = 1500$.

Condition	Method	Parameter	TP	FP	TN	FN
TV12F	TICA	K_e	12	33	0	27
		$K_{\dot{e}}$	41	27	0	4
	MA	K_e	0	15	0	57
		$K_{\dot{e}}$	20	12	0	40
TV12S	TICA	K_e	6	30	0	35
		$K_{\dot{e}}$	41	26	0	4
	MA	K_e	2	10	0	59
		$K_{\dot{e}}$	11	7	0	53

Overall, the example results in Fig. 6 and 7 suggest that detection accuracy is highest based on $K_{\dot{e}}$ for both the TICA and MA methods. Based on the detection results for all runs, all participants, and both the fast and slow CE changes, the final detection accuracy results are summarized in the "confusion matrix" of Table 1. Note that this means a total of 72 data sets were available for each case: 8 participants, 3 repeated runs for 3 different run-in time settings. Here true positives (TP) are successful detections and false negatives (FN) are cases where no detection was triggered. FP and FN are defined as in Section 2.4.

Table 1 shows that for both TV12F and TV12S, the TICA method for detection based on $K_{\dot{e}}$ resulted in the highest number of TPs (41), for a total detection accuracy of 57%. On average, the MA method was found to be less sensitive, with notably less TP and FP detections than TICA, as well as over 70% of cases not triggering a detection (FN). This result is at least partially explained by the heuristic tuning of the hyperparameters. Especially the MA method is highly sensitive to changes in the hyperparameters (especially n_s and ΔT), therefore a much improved result is expected after proper hyperparameter optimization.

4.3 Comparison with Subjective Detection Times

To verify the latency of the adaptation detection, the detection lags for all FP detections were compared with the recorded subjective detection lags (button presses). For the subjective data, statistical analysis with a two-way repeated-measures ANOVA – with G and the added run-in time as factors – showed no difference due to different run-in times, $F(2, 14) = 1.92,\ p > 0.05$. Hence, in the further analysis of detection times, the results of all run-in times were combined. A significant difference was, however, found between TV12F and TV12S, $F(1, 7) = 15.76,\ p < 0.05$, with the sudden change (TV12F) being noted 5 s earlier on average, see Fig. 8.

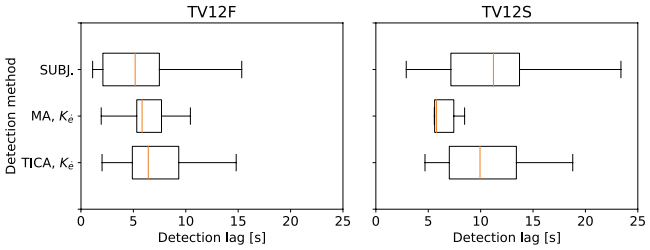

Fig. 8. Lags of true positive detections with MA and TICA compared to subjective detection times (SUBJ.).

Fig. 8 shows the distribution of detection lags, for all TP cases, for the subjective detections ("SUBJ.") and the two tested detection methods ("TICA" and "MA") applied to the identified $K_{\dot{e}}$ data. For TV12F, the detection lags for TICA and MA are found to be equivalent and not significantly different – i.e., $\mathrm{t}(103.1) = -1.62, p > 0.05$ and $\mathrm{t}(66.7) = -0.63, p > 0.05$, respectively – from the subjective data. For the more gradual change in the TV12S condition, all detection lags increase by around 5 s, but still the identification detection lags are equivalent to the subjective data, especially for TICA ($\mathrm{t}(97.0) = 1.42, p > 0.05$). For MA, the 11 FP detections are found to occur a bit earlier on average than the subjective detections, a significant effect $\mathrm{t}(35.0) = 5.13, p < 0.05$.

5. CONCLUSION

This paper tested and compared two methods for the detection of time-varying pilot adaptation from pilot response gain traces estimated online with a recursive ARX identification technique. The methodology was tested on experimental tracking data and identification detection times were explicitly compared to the participants' subjective indication of when they noticed the induced change in the vehicle dynamics. Overall, it was found that identified values of pilot error response gain $K_{\dot{e}}$ showed the most consistent variations due to degraded vehicle stability and hence the most accurate adaptation detection results. The TICA detection method, which checks for differences with *a priori* measured non-adapted pilot behavior, was found to be the most reliable, with a detection accuracy of 57%. The tested MA method, which uses a moving average of the past identified $K_{\dot{e}}$ parameter trace itself as a reference, is more practical for online implementations, but had a lower detection accuracy, which can be improved with better hyperparameter tuning. On average, for offline data processing, the adaptation detection times of both methods were found to be equivalent to the recorded subjective detection lags. Overall, these results indicate that an approach as tested in this paper has the potential to enable accurate and timely detection of pilot adaptations to time-varying adaptations in the controlled vehicle dynamics.

REFERENCES

Boer, E.R. and Kenyon, R.V. (1998). Estimation of Time-Varying Delay Time in Nonstationary Linear Systems: An Approach to Monitor Human Operator Adaptation in Manual Tracking Tasks. *IEEE Trans. on Systems, Man, and Cybernetics – Part A*, 28(1), 89–99.

Duarte, R.F.M., Pool, D.M., van Paassen, M.M., and Mulder, M. (2017). Experimental Scheduling Functions for Global LPV Human Controller Modeling. In *Proc. of the the 20th IFAC World Congress, Toulouse*, 15853–58.

Farjadian, A.B., Annaswamy, A.M., and Woods, D.D. (2016). Towards A Resilient Control Architecture: A Demonstration of Bumpless Re-Engagement Following an Anomaly in Flight Control. In *Proc. of the International Symposium on Sustainable Systems and Technologies, Phoenix (AZ)*.

Hess, R.A. (2009). Modeling Pilot Control Behavior with Sudden Changes in Vehicle Dynamics. *Journal of Aircraft*, 46(5), 1584–1592.

Hess, R.A. (2016). Modeling Human Pilot Adaptation to Flight Control Anomalies and Changing Task Demands. *J. of Guidance, Control, and Dynamics*, 39(3), 655–666.

Ljung, L. (1999). *System Identification – Theory for the User*. Prentice Hall, Inc., second edition.

McRuer, D.T. and Jex, H.R. (1967). A Review of Quasi-Linear Pilot Models. *IEEE Trans. on Human Factors in Electronics*, HFE-8(3), 231–249.

Mulder, M., Pool, D.M., Abbink, D.A., Boer, E.R., Zaal, P.M.T., Drop, F.M., van der El, K., and van Paassen, M.M. (2018). Manual Control Cybernetics: State-of-the-Art and Current Trends. *IEEE Trans. on Human-Machine Systems*, 48(5), 468–485.

Popovici, A., Zaal, P.M.T., and Pool, D.M. (2017). Dual Extended Kalman Filter for the Identification of Time-Varying Human Manual Control Behavior. In *Proc. of the AIAA Modeling and Simulation Technologies Conference, Denver (CO)*, AIAA-2017-3666.

Schiess, J.R. and Roland, V.R. (1975). Kalman Filter Estimation of Human Pilot-Model Parameters. Technical Report NASA-TN-D-8024, NASA Langley Research Center, Hampton (VA).

Thompson, P.M., Klyde, D.H., and Brenner, M.J. (2001). Wavelet-Based Time-Varying Human Operator Models. In *Proc. of the AIAA Atmospheric Flight Mechanics Conference, Montreal (CA)*, AIAA-2001-4009.

van Grootheest, A., Pool, D.M., van Paassen, M.M., and Mulder, M. (2018). Identification of Time-Varying Manual Control Adaptations with Recursive ARX Models. In *Proc. of the AIAA Modeling and Simulation Technologies Conference, Kissimmee (FL)*, AIAA-2018-0118.

Young, L.R. (1969). On Adaptive Manual Control. *Ergonomics*, 12(4), 635–674.

Zaal, P.M.T. (2016). Manual Control Adaptation to Changing Vehicle Dynamics in Roll-Pitch Control Tasks. *Journal of Guidance, Control, and Dynamics*, 39(5), 1046–1058.